Characterization of uranium carbide target materials to produce neutron-rich radioactive beams

Sandrine Tusseau-Nenez [a,*], Brigitte Roussière [a], Nicole Barré-Boscher [a], Alexander Gottberg [b,1], Stefano Corradetti [c], Alberto Andrighetto [c], Maher Cheikh Mhamed [a], Saïd Essabaa [a], Hanna Franberg-Delahaye [d], Joanna Grinyer [d], Loïc Joanny [e], Christophe Lau [a], Joseph Le Lannic [e], Marc Raynaud [a], Abdelhakim Saïd [a], Thierry Stora [b], Olivier Tougait [e]

[a] *Institut de Physique Nucléaire (UMR8608) CNRS/IN2P3 – Université Paris Sud, 91406 Orsay Cedex, France*
[b] *CERN, CH-1211 Genève 23, Switzerland*
[c] *INFN Laboratori Nazionali di Legnaro, Viale dell'Universit'a 2, 35020 Legnaro (PD), Italy*
[d] *Grand Accélérateur National d'Ions Lourds (GANIL), CEA/DSM-CNRS/IN2P3, Bd Henri Becquerel, 14076 Caen, France*
[e] *Institut des Sciences Chimiques de Rennes (UMR 6226) CNRS – Université de Rennes 1, Campus de Beaulieu, 35042 RENNES Cedex, France*

A B S T R A C T

In the framework of a R&D program aiming to develop uranium carbide (UC_x) targets for radioactive nuclear beams, the Institut de Physique Nucléaire d'Orsay (IPNO) has developed an experimental setup to characterize the release of various fission fragments from UC_x samples at high temperature. The results obtained in a previous study have demonstrated the feasibility of the method and started to correlate the structural properties of the samples and their behavior in terms of nuclear reaction product release. In the present study, seven UC_x samples have been systematically characterized in order to better understand the correlation between their physicochemical characteristics and release properties. Two very different samples, the first one composed of dense UC and the second one of highly porous UC_x made of multi-wall carbon nanotubes, were provided by the ActILab (ENSAR) collaboration. The others were synthesized at IPNO. The systems for irradiation and heating necessary for the release studies have been improved with respect to those used in previous studies. The results show that the open porosity is hardly the limiting factor for the fission product release. The homogeneity of the microstructure and the pore size distribution contributes significantly to the increase of the release. The use of carbon nanotubes in place of traditional micrometric graphite particles appears to be promising, even if the homogeneity of the microstructure can still be enhanced.

1. Introduction

Finding optimal properties of the uranium refractory compound target materials constitutes a key ingredient for the production of a wide variety of isotope beams using the ISOL (Isotope Separator Online) technique. Different developments have been achieved in various facilities [1–3] and today uranium carbides with an excess of graphite (with variable stoichiometries, UC_x, since uranium dicarbide UC_2 and uranium monocarbide UC phases can be both stabilized depending on the amount of graphite added) are used by the different operating facilities throughout the world [4–8].

The optimization of UC_x targets is essential for the operation of the next generation facilities: EURISOL, HIE-ISOLDE, SPIRAL2 and SPES. It is also necessary for the existing facilities since higher intensities of short-lived nuclear beams are necessary in order to address important topics in nuclear and astrophysics. Recent experimental research aimed to correlate the submicron-scale porosity of materials with a significant improvement of their release properties. Firstly, very dense UC_x-based targets were developed by hot uniaxial pressing [9–12] and tested: the samples with 20 μm diameter grains of uranium monocarbide (UC) exhibited higher releases for all Rb and Cs isotopes than with a ISOLDE-type target. Then, porous structures were investigated, such as studies at SPES with the use of multi-wall carbon nanotubes (MWCNT) as carbon source [4]. The results showed that the yields were found to be, for most isotopes, lower than those obtained with a standard UC_x target. The microstructure was heterogeneous in term of UC_x grain size (micrometric) and porosity. MWCNT were also tested for other refractory ceramics

* Corresponding author.
[1] Present address: TRIUMF, 4004 Wesbrook Mall, Vancouver, BC V6T 2A3, Canada.

[13,14]. Very recently, a new protocol was developed at ISOLDE and a homogenous nanostructure of LaC_2 was obtained, made of nanometric LaC_2 grains well dispersed in a carbon nanotube fiber matrix that could be stabilized even at high temperature [15].

Radioactive ions beams (RIB) intensities can be increased by improving the release efficiencies of UC_x fission targets which appear clearly correlated to the microstructure of the target material as we have previously shown in the framework of the SPIRAL2 project [7]. This study was dedicated to the development of dense and porous samples, two properties a priori antagonistic but necessary to increase respectively the amount of fission fragments produced and their diffusion out of the target. The quantity of graphite in excess was adjusted to stabilize UC rather than UC_2 in order to increase the density of the target.

The present study is focused on studying the releases out of single pellets of various fission products independently of the ^{238}U concentration. Seven very different UC_x samples ranging from a dense almost monophasic UC sample to highly porous UC_x composites synthesized with carbon nanotubes, instead of graphite, are characterized and compared. The two samples, labeled GATCHINA and CNT in the following, have been provided in the frame of the ActILab project (ENSAR Joint Research Activity within the European 7th Framework Program). The grinding of the uranium precursors and the nature of the carbon source (graphite, microfibers and carbon nanotubes) are taken into account. The whole experimental procedure aims to determine the impact of physico–chemical characteristics of a sample on the release properties. Therefore the correlation between the structural (quantity of phases) and microstructural properties of the samples (grain size, porosity and pore size distribution) and the fission-product release is studied.

2. Preparation and characterization of the samples

2.1. General remarks on techniques and methods used

X-ray diffraction (XRD) patterns were collected by an X-ray powder diffractometer (XRD, D8 Advance, Bruker AXS) in a Bragg–Brentano geometry (θ–θ) equipped with a Cu anode ($K_{\alpha 1}$ = 1.54178 Å). Samples were analyzed in air. Due to the use of a point scintillator detector, long time data acquisition was needed: from 10 to 90° 2θ, 0.02° step size, 16 s/step. Phase identification was performed with the DIFFRACPlus software (version 16, 2013, Bruker AXS) using powder diffraction files (ICDD PDF4+ 2013). The quantitative phase analysis was performed by using the MAUD software [16,17] in order to account for the Cu K_β line (Ni filter, no monochromator) and using the Crystallography Open Database [18]. The instrumental resolution was determined using a LaB_6 NIST standard (Standard Reference Material 660a, cell parameter = 0.41569162 nm ± 0.00000097 nm at 22.5 °C).

The effective density ρ_{eff} of the samples was measured with a helium pycnometer (Accupyc II 1340, Micromeritics). The apparent density ρ_{app} was determined by size measurement while the effective density corresponds to the volumetric mass of the pellet without open porosity [19]. Using these two values of densities, ρ_{eff} and ρ_{app}, the open porosity P_{open} of the samples can be assessed. Theoretical densities (ρ_{theo}) were estimated from the mass fraction of UC, UC_2 and UO_2 obtained by XRD and the estimated carbon in excess after carburization.

The pore size distribution was measured using a mercury intrusion porosimeter (AutoPore IV 9500, Micromeritics). Pressures were increased up to 228 MPa, corresponding to a pore size diameter of 5.5 nm. A surface tension constant of 0.485 N/cm, a contact angle between mercury and the pore wall of 130° were assumed and used in the Washburn equation [20].

The microstructural and morphological features were observed by scanning electron microscopy (SEM – JEOL 6301F) before irradiation. The secondary electron images (predominant topographic contrast) were taken using a 10 kV accelerating voltage. Samples, without metallization and polishing, were observed on both surface and fracture.

2.2. Characterizations of the raw powders

2.2.1. Uranium precursors

Depleted (0.3 wt% ^{235}U) uranium dioxide powder from CEA Cadarache (reference MN371) was used at the ALTO facility until March 2013. Hereafter AREVA depleted (0.25 wt% ^{235}U) uranium dioxide (MN894) is used; the powder consists of agglomerates made of spherical grains with an average size about 100 nm. The depleted uranium dioxide powder (0.31 wt% ^{235}U) used for samples prepared at ISOLDE-CERN is supplied by Westinghouse with an average particle size of 16 μm. The uranium oxalate powder, $U(C_2O_4)_2$, $2H_2O$, was prepared at IPNO [21,22] from uranium chloride obtained by dissolving natural metallic uranium in concentrated (4 M) hydrochloric acid; the powder consists of cuboid grains, with an average size of 2 μm.

2.2.2. Carbon precursors

The graphite powder (Cerac, purity = 99.5%, 325 mesh) was observed by SEM: it exhibits a large grain size distribution with a diameter less than 40 μm. SEM observations on carbon microfibers (Torayca) reveal a diameter of 5.2–7.5 μm with a length ranging from 55 to 310 μm, while the purchaser indicates a diameter of 7 μm and a length ranging from 10 to 150 μm. MWCNT were purchased from Nanocyl SA, (>95% C, <5% Metal Oxide, D = 9.5 nm, L = 1.5–10 μm) and used as received.

2.3. Synthesis of the pellets

The OXA samples were prepared from a mixture of uranium oxalate and graphite with a ratio of 1 mol of UO_2 for 3 mol of graphite. The COMP30 samples consisted of OXA samples in which 30 wt% of microfibers (μC) was added. Several mixtures were done separately and mixed together in order to obtain one homogeneous mixture for the preparation of the pellets. One batch for one pellet weighted about 1.3 g to obtain after sintering a pellet of about 1 g.

The UO_2 powders used at IPNO were ground before use with a mixer mill RETSCH PM200 or a planetary mill RETSCH PM100. The UO_2 for CNT samples provided by CERN was used as supplied.

GATCHINA pellets were obtained by powder metallurgy from uranium and graphite, as previously published [9–12]. The pellets used in this work presented an apparent density of 12.7 g cm^{-3} and an average grain size of 6 μm. Information about the raw powders was not available.

The experimental setups are summarized in Table 1. Table 2 summarizes the conditions of synthesis of the seven kinds of tested samples. At IPNO, UO_2 and graphite were mixed together manually in an agate mortar. At CERN, depleted UO_2 powder with an average particle size of 16 μm was mixed with MWCNT (9.5 nm thickness and 1.5–10 μm length) in a vibratory ball mill.

2.4. Pressing

A semi-automatic hydraulic press placed in a glove box was used (SPECAC Automatic Hydraulic Press) for OXA, COMP30 and PARRNe samples. The pressing protocol was performed by steps: from 0 to 3 t, waiting 1 min; from 3 to 5 t, waiting 3 min; from 5 to 7.5 t, waiting 1 min; from 7.5 to 10 t, waiting 15 min and after a slow decrease of the pressure. A 13 mm or 14 mm diameter pellet

Table 1
Experimental setups for the milling of uranium oxide.

Miller type	Balls type	Diameter of balls (mm)	Number of balls	UO_2 mass (g)	Liquid volume (mL)	Milling time (min)	Frequency (Hz)
Mixer	Inox	9	6	2×10	0	30	30
Planetary	Inox	3	600	36.68	16	60	5.5

Table 2
Summary of the synthesis.

Sample	Uranium source	Carbon	C/U	UO_2 milling
OXA	IPNO oxalate, natural U	Graphite	3	
COMP30	IPNO oxalate, natural U	Graphite + 30 wt% of microfibres	4	
PARRNe 371	UO_2, depleted U 0.3%	Graphite	6	Mixer
PARRNe 894	UO_2, depleted U 0.25%	Graphite	6	Mixer
PARRNe 894BP	UO_2, depleted U 0.25%	Graphite	6	Planetary
CNT	UO_2, depleted U 0.31%	Carbon nanotubes	6	No
GATCHINA	U	Graphite	1	

die was used, leading to a final applied pressure respectively of 740 or 640 MPa.

For CNT, 14 mm diameter die was used and pressed at 510 MPa. The protocol was similar to that described for lanthanum carbide [23].

2.5. Carburization

For GATCHINA, information about temperature of sintering and applied pressure for the hot uniaxial pressing (HUP) were not reported. The reaction was:

$$U + C \rightarrow UC \quad (1)$$

According to a recent study [24], the use of vacuum for carboreduction favors the release of CO instead of CO_2, even if a small release of CO_2 was observed. Nevertheless, concerning the uranium oxalate dihydrate, the CO_2 release cannot be avoided as it was reported in [21] by TG/TD analyses under inert atmosphere and the expected equations were:

$$\text{For OXA}: U(C_2O4)_2, 2H_2O + 3C \rightarrow UC + 2CO_{2(g)} + 4CO(g) + 2H_2O_{(g)} \quad (2)$$

$$\text{For COMP30}: U(C_2O_4)_2, 2H_2O + 3C + \mu C \rightarrow UC + 2CO_{2(g)} + 4CO_{(g)} + 2H_2O_{(g)} + \mu C \quad (3)$$

$$\text{For the other samples}: UO_2 + 6C \rightarrow UC_2 + 2CO_{(g)} + 2C \quad (4)$$

The carburization was performed under a secondary vacuum (typically 10^{-3} Pa) with a heating rate of 2 °C/min and a plateau of 16 h at 1770 °C. The heating was controlled by the pressure, the next heating step (10 A each 10 min) was not performed until the pressure was under 2.10^{-2} Pa.

Green CNT samples were prepared at CERN and carburized at IPNO before the irradiation tests. The carburization plateau was 20 min after which the furnace broke. The release measurements of CNT samples were performed, but it is important to keep in mind a reduced duration of the plateau, inducing a potentially limiting grain growth and a low densification compared to the other samples.

2.6. Physicochemical characterizations of the sintered pellets

2.6.1. Phase identification and quantification

The selected ICDD patterns for the identification of phases by XRD and Rietveld refinements are summarized in Table 3. First bulk pellets were analyzed by XRD. Then, they were ground, under Ar atmosphere, to powder in a agate mortar for comparison.

For the GATCHINA sample, the grinding of the pellet is expected to release the microstrain relaxation induced by the HUP sintering. Analyzing the bulk leads to broad Bragg lines whereas powder leads peaks at the same positions but with a reduced broadening, for example the full width at half maximum (FWHM) is reduced from 0.4508 °2θ to 0.1771 °2θ for the (1 1 1) Bragg line. For PARRNe 894BP and PARRNe 894 samples, the comparison of the bulk and powder patterns shows a sensitivity of the (0 0 l) planes of graphite, whereas the relative intensities of UC and UC_2 Bragg lines are not impacted. As expected, the graphite is textured due to the pressing of the pellet before sintering, the observed intensities are higher than expected. For OXA, which exhibits only UC and UC_2 phases, the pressing does not induce texture, the observed intensities match the ICDD patterns.

Fig. 1 shows the XRD patterns obtained for 5 ground samples, namely PARRNe 894BP, PARRNe 894, GATCHINA, OXA and COMP30. Table 4 summarizes the uranium phase identification for the 7 types of samples. As expected from Eqs. (1)–(4), OXA and GATCHINA samples are mainly made of UC, however a low

Table 3
Crystallographic data on synthesized phases for phase identification and Rietveld refinements.

Phase	Space group	Cell parameters (Å)	Atomic positions	Theoretical density	ICDD Pattern	Refs.
UC	Fm-3 m (225)	a = 4.9590	U 4a 0 0 0 C 4b ½ ½ ½	13.65	96-900-8757	[25–27]
α-UC_2	I4/mmm (139)	a = 3.5090 c = 5.9800	U 2a 0 0 0 C 4e 0 0 0.388	11.75	01-084-1344	[25–27]
Graphite	P 63 mc (186)	a = 2.4610 c = 6.7080	C 2a 0 0 0 C 2b 1/3 1/3 0.005	2.26	96-901-2231	[28]
UO_2	Fm-3 m (225)	a = 5,4680 Å	U 4a 0 0 0 C 8c 1/4 1/4 1/4	10.90	01-075-0455	[29]

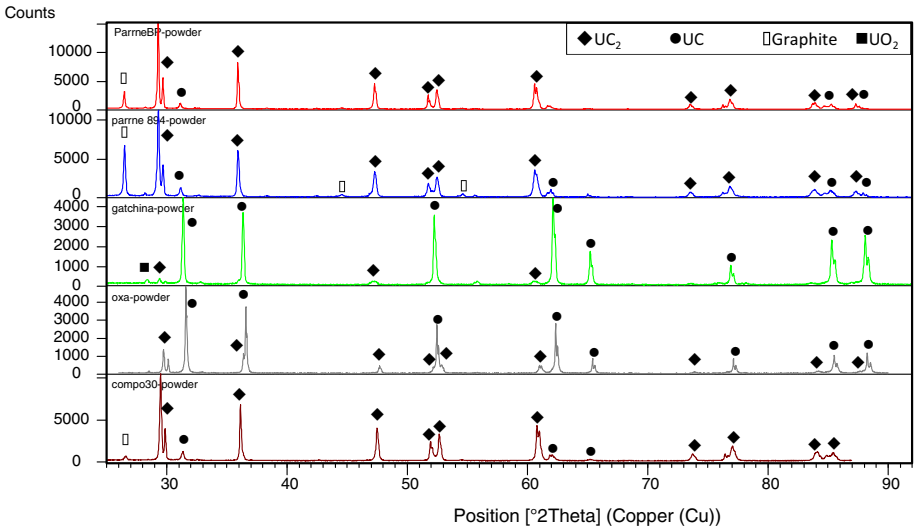

Fig. 1. XRD phase identification for ground pellets.

Table 4
Rietveld analysis. The sum of the relative proportions of UC, UC_2 and UO_2 is equal to 100%.

Sample	Identified phases	Cell parameter (Å)	Quantitative analysis (wt.%)
OXA	UC	a = 4.9614	70.5
	UC_2	a = 3.5286, c = 6.0104	29.5
COMP30	UC	a = 4.9590	8.6
	UC_2	a = 3.5215, c = 5.9969	91.4
PARRNe 371	UC	a = 4.9624	10.6
	UC_2	a = 3.5236, c = 5.9953	89.4
PARRNe 894	UC	a = 4.9556	10.5
	UC_2	a = 3.5249, c = 6.0006	85.9
	UO_2	a = 5.4680	3.6
PARRNe 894BP	UC	a = 4.9565	5.8
	UC_2	a = 3.5230, c = 5.9980	94.2
CNT	UC	a = 4.9616	14.7
	UC_2	a = 3.5232, c = 5.9928	85.3
GATCHINA	UC	a = 4.9567	86.9
	UC_2	a = 3.5398, c = 6.0055	8.6
	UO_2	a = 5.4653	4.5

quantity of UC was turned into UC_2. No graphite is observed for GATCHINA and OXA, indicating that its quantity is less than about 1–2 wt%. For COMP30, UC is expected whereas UC, UC_2 and graphite are observed showing that the microfibers react with uranium dioxide. For PARRNe samples, UC_2, UC and graphite are clearly identified. Sometimes, UO_2 is observed due to the oxidation of the surface of the pellet, despite all sample-preparation precautions. Indeed, the pyrophoricity of UC induces the formation of UO_2 when pellets are ground to powder, more sensitive to air.

For OXA sintered sample, XRD analysis shows no excess of graphite or UO_2. This indicates that the reaction between 1 mol of oxalate and 3 mol of graphite (experimentally introduced) was complete. Considering only CO degassing induces the hypothesis of 4 mol of graphite introduced as precursors. In this case, all the uranium phase does not react and residual uranium oxide peak should have been observed by XRD. According to [21], CO and CO_2 degassing should be considered and Eqs. (1)–(4) should be rewritten as follows:

$$\text{For GATCHINA}: \ \mathrm{U} + (1+x)\mathrm{C} \rightarrow (1-x)\mathrm{UC} + x\mathrm{UC_2} \tag{5}$$

$$\text{For OXA}: \mathrm{U(C_2O_4)_2, 2H_2O} + 3\mathrm{C} \rightarrow x\mathrm{UC} + (1-x)\mathrm{UC_2} + x\mathrm{C} + 2\mathrm{CO_{(g)}} + 3\mathrm{CO_{2(g)}} + 2\mathrm{H_2O_{(g)}} \tag{6}$$

For COMP30, microfibers reacted with uranium oxalate leading to the formation of UC_2, the equation should be, assuming graphite and microfibers as carbon:

$$\mathrm{U(C_2O_4)_2, 2H_2O} + 4\mathrm{C} \rightarrow (1-x)\mathrm{UC_2} + x\mathrm{UC} + x\mathrm{C} + 4\mathrm{CO_{(g)}} + 2\mathrm{CO_{2(g)}} + 2\mathrm{H_2O_{(g)}} \tag{7}$$

For the other samples, the carburization reaction could be described by:

$$\mathrm{UO_2} + 6\mathrm{C} \rightarrow x\mathrm{UC_2} + (1-x)\mathrm{UC} + (3-x)\mathrm{C} + 2\mathrm{CO_{(g)}}. \tag{8}$$

To be able to perform the quantitative phase analysis by the Rietveld method, the grinding of pellets is required. However CNT and PARRNe 371 were not ground because only few samples were available for all studies but, as mentioned above for PARRNe 894BP and PARRNe 894, the relative UC/UC_2 ratio is not sensitive to the nature (bulk or powder) of the sample.

Because of the texture, only (002) and (004) lines are observed for graphite; which is not enough for the Rietveld refinement [30]. In consequence, as the Bragg lines of graphite do not overlap with those of other phases, it was decided to exclude it from the Rietveld calculations.

The crystallographic models chosen for this study are summarized in Table 3. Several R-factors are commonly used to evaluate the fit quality [31], as:

- The weighted profile R-factor, R_w, corresponding to the square root of the minimized quantity scaled by the weighted intensities. This factor takes into account the background of the pattern and indicates the quality of the profile fitting. R_w should be less than 15%.
- The expected R-factor, R_{exp}, corresponds to the best possible Rw.
- The goodness of fit (GOF), χ^2 or σ (for Maud software), which is $\chi^2 = (R_w/R_{exp})^2$. A good refinement gives value lower than 2.
- The Bragg R-factor, indicating the deviation between observed and calculated intensities of Bragg lines. It indicates the quality of the structural model and should be less than 20%.

- The Rietveld refinement for LaB_6 NIST standard leads to satisfactory agreement factors (R_w = 8.9%, R_{exp} = 6.8%, σ = 1.3, and R_B = 6.6%) in view of the instrumental conditions. All the results are summarized in Table 4.

For all the samples, the agreement factors were in the ranges: 9.0% < R_w < 13.9%, 5.5% < R_{exp} < 8.8%, 1.3 < σ < 2.3, and 6.6% < R_B < 18.7%.

For UC and UC_2, the calculated cell parameters are in agreement with the literature data review of Chevalier and Fischer [26]. Even if U and C are mixed in stoichiometric proportion to synthesize UC, as in the case of OXA and GATCHINA, UC and UC_2 are obtained. For OXA, this significant quantity of UC_2 could be attributed to the uranium oxalate precursor used. Actually Hy et al. [7] showed that UC_2 was obtained by using uranium oxalate and was not observed by arc-melting of uranium and graphite powders. The reduction of the UO_2 grain size (planetary milling) seems to favor UC_2 stabilization (95 wt% of UC_2 in PARRNe 894BP), maybe due to the higher homogeneity of the powder particle size.

UC_2 Bragg lines exhibit 2-fold FWHM compared to the LaB_6 reference sample, while FWHM for UC are even four times broader. Nevertheless, considering the carburization conditions, these FWHM cannot be attributed to a nanometric crystallite size effect. The hypothesis of dissolution of oxygen according to Tawaga and Fujii [32] also is not in agreement with the present calculated cell parameters. These large FWHM could be explained by the present elaboration conditions corresponding to the two-phase field domain in the U–C phase diagram [26], leading to a continuous change in the cell parameters and microstrains due to the distortion between the cubic (UC) and tetragonal (UC_2) lattices.

2.6.2. Density and porosity

The quantity of carbon source (graphite, MWCNT or microfibers) could be deduced from the molar ratio of UC and UC_2 according to the Eqs. (5)–(8).

For each type of sample, 3–5 pellets were analyzed by He pycnometry. These systematic measurements have allowed estimating the error bars. All samples were analyzed before and after carburization, only the GATCHINA samples were already received in the carburized state. The average values obtained for porosity and density are given in Table 5.

Except for PARRNe 894 that tends to swell, shrinkage occurs during the carburization process despite the degassing.

GATCHINA is obviously dense (effective density of 13.1 g cm^{-3} to be compared with the theoretical value of 13.65 g cm^{-3} for UC) and has a 5% open porosity. The apparent density, 12.4 g cm^{-3}, is in agreement with published data [9–12].

OXA and COMP30, made from uranium oxalate, shrunk by about 80% leading to the lowest open porosity for OXA. For COMP30, the open porosity is comparable to the PARRNe samples and can be ascribed to the use of microfibers and the effective density is still high. Nevertheless, the closed porosity reaches more than 10%, maybe due to the transformation of oxalate into oxide. PARRNe 894BP and 371 have the same characteristics. The grinding by planetary milling, more efficient, leads to smaller grains of UO_2 consequently the shrinkage increases while the open and closed porosities remain at 45% and less than 5% respectively. In comparison, using MWCNT instead of graphite leads to similar shrinkage and effective density whereas the open porosity reaches 80% while keeping 5% of closed porosity.

2.6.3. Pore size distribution

Six types of samples were analyzed by mercury porosimetry (Table 6). The GATCHINA one was not characterized because of its low open porosity. The results from heat-treated graphite are added in order to compare with the signal from the graphite included eventually in the tested samples. The normalized open porosity volume ($cm^3\ g^{-1}$) obtained by He pycnometry is also reported in Table 6, to allow the comparison with the normalized total pore volume, i.e. the total mercury volume introduced by

Table 5
Density and porosity derived from Helium pycnometry on samples before and after carburization. Shrinkage deduced from geometrical measurements. Error bars are indicated in parentheses.

Sample	Carburization	Shrinkage (%, ±2)	Theoretical density (g cm^{-3})	Apparent density (g cm^{-3}, ±0.2)	Effective density (g cm^{-3}, ±0.2)	Open porosity (%, ±3)	Closed porosity (%, ±3)
OXA	Before	85	3.42	2.5	3.1	17	10
	After		13.03	8.7	12.2	26	7
COMP30	Before	75	3.38	2.4	3.2	26	4
	After		11.69	4.5	10.1	48	13
PARRNe 371	Before	10	6.18	4.6	6.0	23	3
	After		8.65	4.4	8.3	46	4
PARRNe 894	Before	⩽0	6.18	4.9	5.8	15	5
	After		8.65	3.1	8.0	56	8
PARRNe 894BP	Before	20	6.18	3.9	5.9	32	4
	After		8.67	4.4	8.2	44	6
CNT	Before	17	6.18	1.5	5.8	70	6
	After		8.93	1.6	8.5	77	5
GATCHINA	Before		–	–	–	–	–
	After		13.37	12.4	13.1	5	2

Table 6
Summary of the open porosity characteristics: open pore volume from He pycnometry and total pore volume and area from Hg porosimetry.

	OXA	COMP30	PARRNe 371	PARRNe 894	PARRNe 894BP	CNT	Graphite
Open pore volume per gram ($cm^3 \cdot g^{-1}$, ±0.005)	0.027	0.108	0.101	0.176	0.099	0.454	0.104
Total pore volume per gram, ($cm^3 \cdot g^{-1}$)	0.017	0.111	0.097	0.160	0.090	0.427	0.104
Total pore area ($m^2 \cdot g^{-1}$)	0.271	0.584	0.750	0.776	0.633	14.887	6.793

mass of sample. These two results, both reflecting the total open pore volume, are consistent, which indicates the reliability of the two methods. The total pore area is similar for all the samples, except for OXA and CNT, where the areas are found to be reduced by half and increased 20 times respectively. These behaviors can be correlated with the 85% shrinkage and the high effective density in the case of OXA and with the use of MWCNT and the reduced carburization plateau.

The pore size diameter distributions of all the samples are shown in Fig. 2. The largest pores are described by the logarithmic differential intrusion curve. Graphite has no pore in the 0.8–400 μm range. CNT, very porous, exhibits an intense peak in the range of 10–30 μm. For the others, the intensity of the more intense peaks is 5- to 10-fold lower. Few pores with a diameter between 1 and 2 μm are observed for OXA. The pore size of PARRNe 894 is very heterogeneous, with a pore diameter distribution between 300 nm and 200 μm. Only samples from mixer milled powders (PARRNe 371 and 894), and to a lesser extent with microfibers, have pores larger than 100 μm. Pore diameters in the range of 1–10 μm are observed for CNT, COMP30, PARRNe 894BP and 371.

Fig. 2 describes also the smaller pore size diameters by the differential intrusion curve. As expected, CNT exhibits intense peaks in the range of 10–100 nm, 3 times more intense than graphite. The intrinsic pores of graphite remain in the respective samples. Pore size diameters less than 1 μm is attributed only to the source of carbon used.

2.6.4. Microstructure

SEM, in secondary electron mode, was used for the qualitative description of the microstructures. The GATCHINA pellet morphology (Fig. 3) is different than the others, due to the HUP sintering. The surface seems flattened and dense. At higher magnification, one can observe very dense zones with few pores and some porous zones made of submicrometric UC grains. On fracture, only dense parts are observed. These observations are in agreement with the 5% of open porosity measured by He pycnometry.

The samples obtained by conventional carburization are macroscopically different (Figs. 4 and 5). The observed morphologies are similar on surface (Fig. 4) and on fracture (Fig. 5) for each of the six samples.

Cracks are clearly observed on OXA, COMP30 and PARRNE 894 and can be correlated with the 100 μm pores obtained by Hg porosimetry. The homogeneity of PARRNe 894BP is obvious, using planetary milled UO_2 powder homogenizes the microstructure avoiding large pores. CNT and PARRNe 894 are the most porous samples, which is in agreement with He pycnometry measurements above.

OXA exhibits the most homogeneous microstructure without excess of graphite. Few pores of about 1–2 μm diameter are dispersed around the grains. This UC_x intergranular porosity corresponds to the pore size diameter in the range 1–10 μm observed by Hg porosimetry.

For COMP30, three zones are observed. The first one, porous, is composed of micrometric grains of UC_x forming agglomerates, the

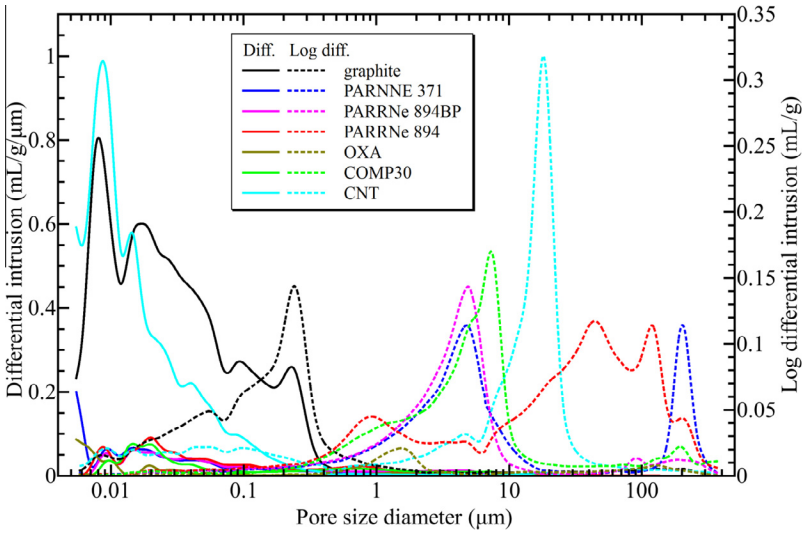

Fig. 2. Pore size diameter distribution obtained by Hg porosimetry. For CNT, differential and log differential intrusions represented in this figure were divided by a factor 3.

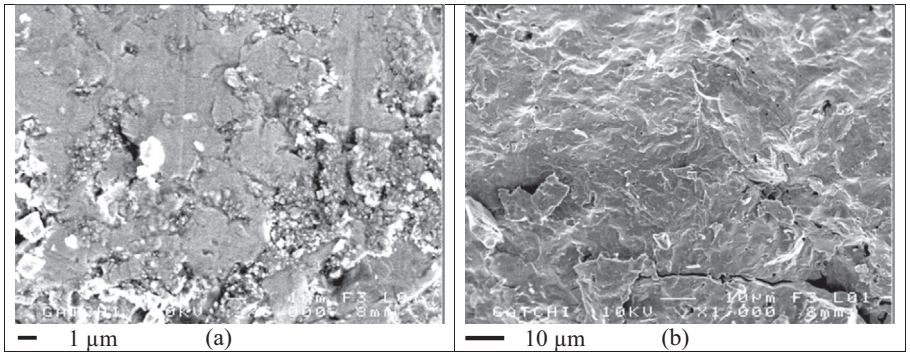

Fig. 3. Observations on the GATCHINA pellet by SEM, (a) surface (magnification × 5000), (b) fracture (magnification × 1000).

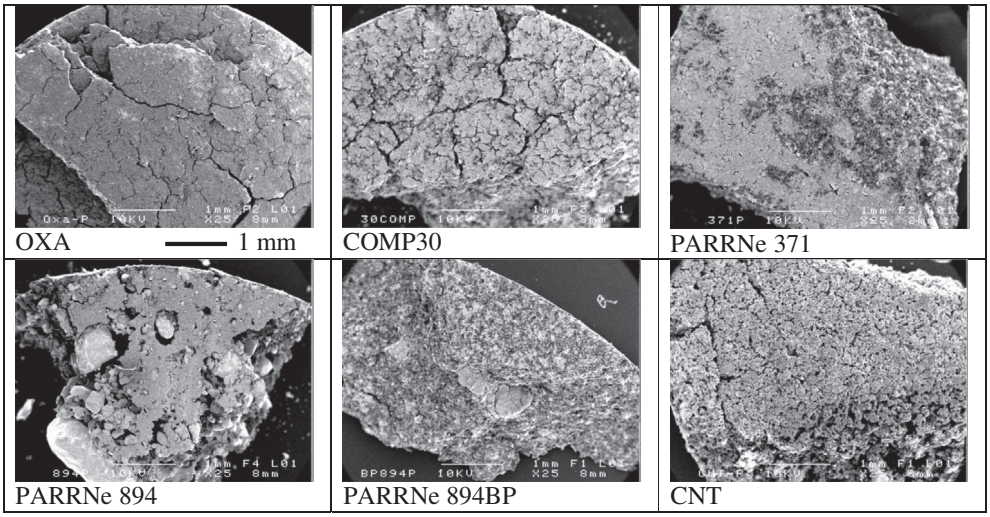

Fig. 4. SEM large scale observation on pellet surface (same magnification, ×25).

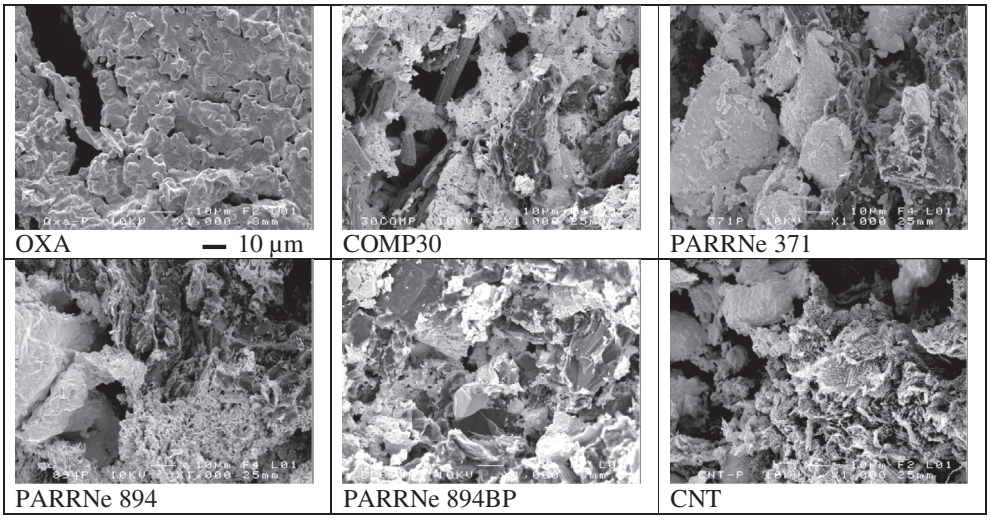

Fig. 5. Observations at induced pellet fractures. Zones that are rich of UC_x appear bright while those carbon rich appear darker (same magnification, ×1000).

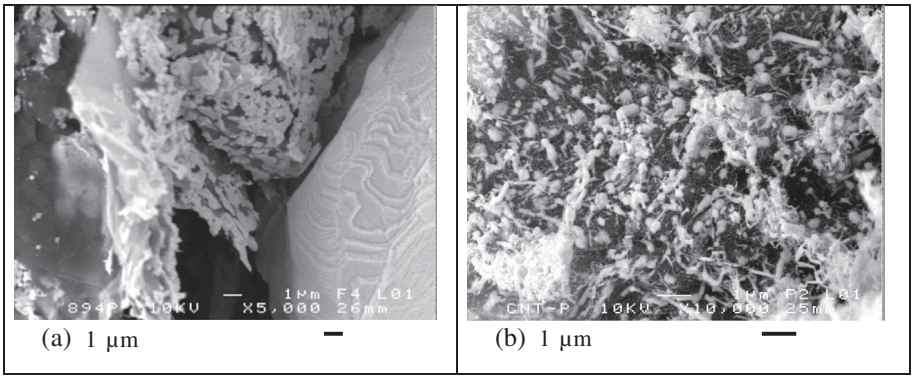

Fig. 6. Growth of UC_x on (a) graphite sheets observed for PARRNe 894, (b) on nanotubes for CNT.

second one is made of a mixture of graphite sheets and UC_x micrometric grains, and the third one corresponds to large pores where microfibers can be observed. For PARRNe 371, large agglomerates of UC_x grains (up to 40 µm) are embedded in the typical mixture of graphite and micrometric grains of UC_x. UC_x grain growth on graphite foils can be observed (Fig. 6a). For PARRNe 894, the size of agglomerates can reach up to 1 mm. Zones rich of UC_x are more porous than in PARRNe 371. PARRNe 894BP is less porous than 894, as shown by He pycnometry. However, large agglomerates are still observed but with a reduced size, like in PARRNe 371.

The porous microstructure of CNT comprises agglomerates about 20 μm made of UC_x micrometric grains and some clusters of MWCNT on which UC_x growth is observed (Fig. 6b). The UC_x agglomerates appear to be smaller than in PARRNe type samples.

All these physicochemical characterizations lead us to conclude that the grinding of uranium dioxide improves the homogeneity of the microstructure after carburization. Of course, the shrinkage is increased but the open porosity is still high. The carburization of ground powder, following Eq. (8), tends to stabilize mostly UC_2. Using uranium oxalate instead of uranium dioxide as precursor favors degassing during carburization but against prediction, these samples exhibit the largest fraction of closed porosity. The effective density is higher even if graphite is in excess (compare COMP30 with PARRNe-type samples). Using microfibers favors the formation of very large pores (see cracks on pellet surface) but the average open porosity is not increased in comparison with the samples made of graphite only. The use of MWCNT improves the open porosity significantly. The microstructure of the pellet is more homogeneous with a limited grain growth. Nevertheless, it should be noted that, for the CNT pellets, the carburization lasted only 20 min, instead of 16 h for the other samples.

3. Release measurements

3.1. Experimental procedure

The release properties of the different uranium carbide samples were obtained applying the procedure described previously [7]. ^{238}U fission was induced by fast neutrons. The neutrons, in turn, were generated by break-up reactions of a 20 nA, 27 MeV deuteron beam delivered by the ALTO facility impinging onto a converter, consisting of a graphite disc positioned just in front of the target pellets. The release fractions were determined by comparing the intensity of specific gamma transitions found in a heat treated sample, compared to a sample left at room temperature for the same duration. A new irradiation station and a new sample holder, containing the two pellets and the graphite converter, have been designed. This device is mechanically adjusted in order to get accurate and reproducible positions of the deuteron beam on the graphite converter.

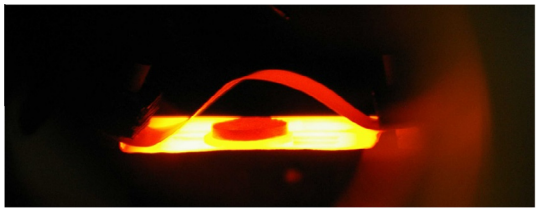

Fig. 7. Tantalum furnace with tantalum cover foil and graphite pellet.

For the heating procedure, a new vacuum furnace was developed to avoid any oxidation of the pellet during the process, to keep the mechanical strength of the pellet. The oven consists of a tantalum boat (63 mm length and 25 mm width) covered by a tantalum foil with the same dimensions, acting as heat shield (Fig. 7). Given the reduced dimensions of the furnace, the temperature can be assumed uniform in the sample. Between the tantalum boat and the uranium carbide pellet, a graphite pellet of 1.5 mm is interposed to avoid chemical reactions between tantalum and uranium carbide materials. The temperature was controlled by a monochromatic pyrometer (IMPAC IGA 140 equipped with a thru-lens view finder and a set emissivity $\varepsilon = 0.877$) and the observation of the internal platinum melting. The melting of about 0.01 g of Pt placed on the graphite pellet indicated the intended temperature, i.e. 1768 °C. The recorded pressure in the furnace at this temperature was from 1.5 to 5.10^{-2} Pa. According to the tabulated data for the vapor pressure of Pt [33], at this pressure Pt evaporates at respectively 1671 °C and 1744 °C. Experimentally, clearly the deposition of Pt was observed on window furnace, a cleaning was needed. In the following, we consider that an average heating temperature of 1700 °C was reached.

The main features of this oven are a very fast temperature slope while heating and cooling (about 7 min from 20 °C to 1700 °C). The observed cooling time of heated pellets was about 6 min and argon was used in order to increase the cooling by convection in the gas. The handling temperature of the pellet was less than 40 °C which is a safe level to avoid the pyrophoric behavior in air.

Table 7 shows the release measurements performed: for each sample, the irradiation time as well as the heating and γ-measurement conditions are indicated. The first γ measurement is used to determine the ratio between the activities of the two pellets and the second one to obtain the released fractions (RF) from the comparison of the intensities of the γ transitions emitted by the heated and non-heated samples. The procedure for determining the released fractions and their associated error bars is described in details in Ref. [7].

3.2. Release results

Fig. 8 shows the γ spectra obtained in the 1750–2550 keV energy range of all samples after heating as well as those of non-heated GATCHINA and CNT samples. These γ spectra were normalized in order to correct from the yield differences between the samples. They exhibit γ transitions belonging to the ^{88}Kr, ^{88}Rb, $^{134,135}I$, ^{138}Cs and ^{142}La decays and already indicating that the

Table 7
Experimental conditions of the release measurements. The waiting time is the time between the end of the irradiation and the beginning of the measurement.

Sample	Irradiation	1st γ measurement		Heating		2nd γ measurement	
	t (m)	$t_{waiting}$ (m)	$t_{counting}$ (m)	T (°C)	t (m)	$t_{waiting}$ (h:m)	$t_{counting}$ (m)
CNT	20	29	10	1700	30	1:31	60
COMP30	20	40	10	1700	30	1:55	60
GATCHINA	10	31	10	1700	30	1:48	60
	10	29	10	2000	30	1:39	60
OXA	20	31	10	1694	30	1:41	60
PARRNe 371	20	29	10	1500	60	1:59	60
	20	41	10	1650	30	1:45	60
	20	60	10	1700	15	1:48	60
	20	25	10	1700	30	1:30	60
	20	38	10	1700	60	2:38	60
PARRNe 894	20	34	10	1600	10	2:15	60
				1500	20		
PARRNe 894BP	20	36	10	1700	30	1:38	60

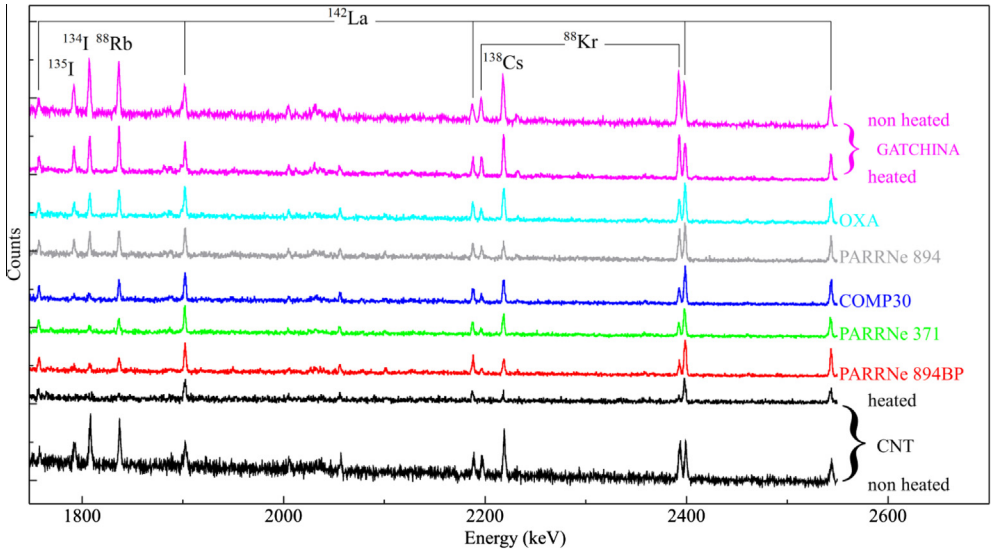

Fig. 8. Partial γ-ray spectra obtained with the different UC_x pellets before or after heating. All the pellets have been heated at 1700 °C during 30 min, except the PARRNe 894 one heated at 1600 °C during 10 min then at 1500 °C during 20 min.

release properties vary strongly with the type of UC_x. With the GATCHINA pellets, even the most volatile elements like Kr and I strongly remain present after heating. For instance, one can note that, in the doublet located at 2400 keV, the γ-transition belonging to the ^{88}Kr decay is stronger than the peak resulting from the ^{142}La decay, contrary to what is observed with the other samples. After heating, the CNT sample exhibits peaks with very weak intensities and contains almost any ^{142}La. Thus from these spectra, the released fractions are low for the GATCHINA sample while they are very high for the CNT. In order to confirm or infirm the release behavior of the GATCHINA pellets, another measurement has been performed heating the pellet to 2000 °C, the target temperature most often used during on-line experiments.

Fig. 9 shows the fraction released by the seven samples for thirteen elements, namely Kr, Sr, Y, Ru, Sn, Sb, Te, I, Xe, Cs, Ba, La, Ce. These released fractions have been obtained from the γ-spectroscopy measurements following the procedure described by Hy et al. [7]. The noble gases, Kr (Z = 36) and Xe (Z = 54), are well released by the different UC_x samples, except for GATCHINA. After heating at 1700 °C, the Kr released fractions (RF) are greater than 80% for CNT, between 60 and 70% for PARRNe 894BP, PARRNe 371 and COMP30. They drop to 50% for OXA and are lower than 10% for GATCHINA. With the latter, the only element for which the released fraction reached 60% is Sn. One can note that the dominant process controlling the fission-product release by UC_x targets is diffusion for noble gases whereas it is desorption or effusion for Sn [34]. The low release properties of the GATCHINA-type uranium carbide are confirmed by the measurement performed after heating the pellet to 2000 °C since the RF values obtained at 2000 °C are only slightly better than or equal to (in the limits of error bars) those measured at 1700 °C. Both measurements, at 1700 °C and 2000 °C, can be considered as a conclusive test of reproducibility of the release properties for the GATCHINA-type UC_x pellets.

The effects of two parameters, heating temperature and heating time, on the released fractions (RF) have been studied using PARRNe 371 samples. The results are shown in Fig. 10. The RF have been determined for three heating temperatures (1500, 1650 and 1700 °C) and three heating times (15, 30 and 60 min). In Fig. 10A, two data sets are presented: the first one was obtained after heating a pellet to 1700 °C for 30 min, the second one after heating a pellet to 1650 °C for the same time. For almost all elements, no dependence upon the heating temperature is observed. The RF measured at 1650 °C are slightly lower than the values obtained at 1700 °C only for Sr (Z = 38), Xe (Z = 54) and Ba (Z = 56). As the difference in temperature is small (50 °C), one can wonder whether the RF variations observed are really significant or rather reveal the dispersion in performance of different samples that are otherwise assumed identical (since they are manufactured in the same way). Fig. 10B shows the results obtained after heating pellets to 1700 or 1500 °C for 60 min: the RF values in both cases are very similar for all studied elements, within the error bars. The three data sets presented in Fig. 10C correspond to samples heated to 1700 °C for 15, 30 and 60 min. The RF measured do not seem to depend on the heating time. Indeed, only for two elements, namely Y (Z = 39) and Te (Z = 52), the error bars do not overlap but the dispersion is not greater than that observed in Fig. 10A, where it could result from sample variations. It appears therefore that the release time (time until no significant release is observed) for most of studied elements is less than 15 min. Within the heating temperature and time ranges studied, the reproducibility of the release properties is demonstrated for the PARRNe 371 sample: the shapes defined by the lines linking the RF values are very similar for the five measurements performed. Moreover this shape differs strongly from that obtained from the other types of uranium carbide (see Fig. 9).

From the γ-spectrometry measurements, we can conclude that the RF depend strongly on the type of UC_x and only very slightly on the heating temperatures and heating times, at least within the ranges studied here. The release results have been found to be reproducible for all samples that have been studied repetitively (GATCHINA and PARRNe 371) and finally, the shape obtained for the RF as a function of the atomic number Z (Fig. 9) can be considered as the release fingerprint of each UC_x sample.

4. Discussion

Fig. 11 shows the RF of the seven UC_x samples as a function of the boiling temperature at 5×10^{-5} mbar for the various elements studied. Cerium, lanthanum and ruthenium are poorly released by all samples; in case of Ce and La, this resistance to release is attributed to the chemical analogy of lanthanides with uranium [7] whereas in case of Ru, it is considered to be a result of the refractory nature of this element. Fig. 11 can be used to classify

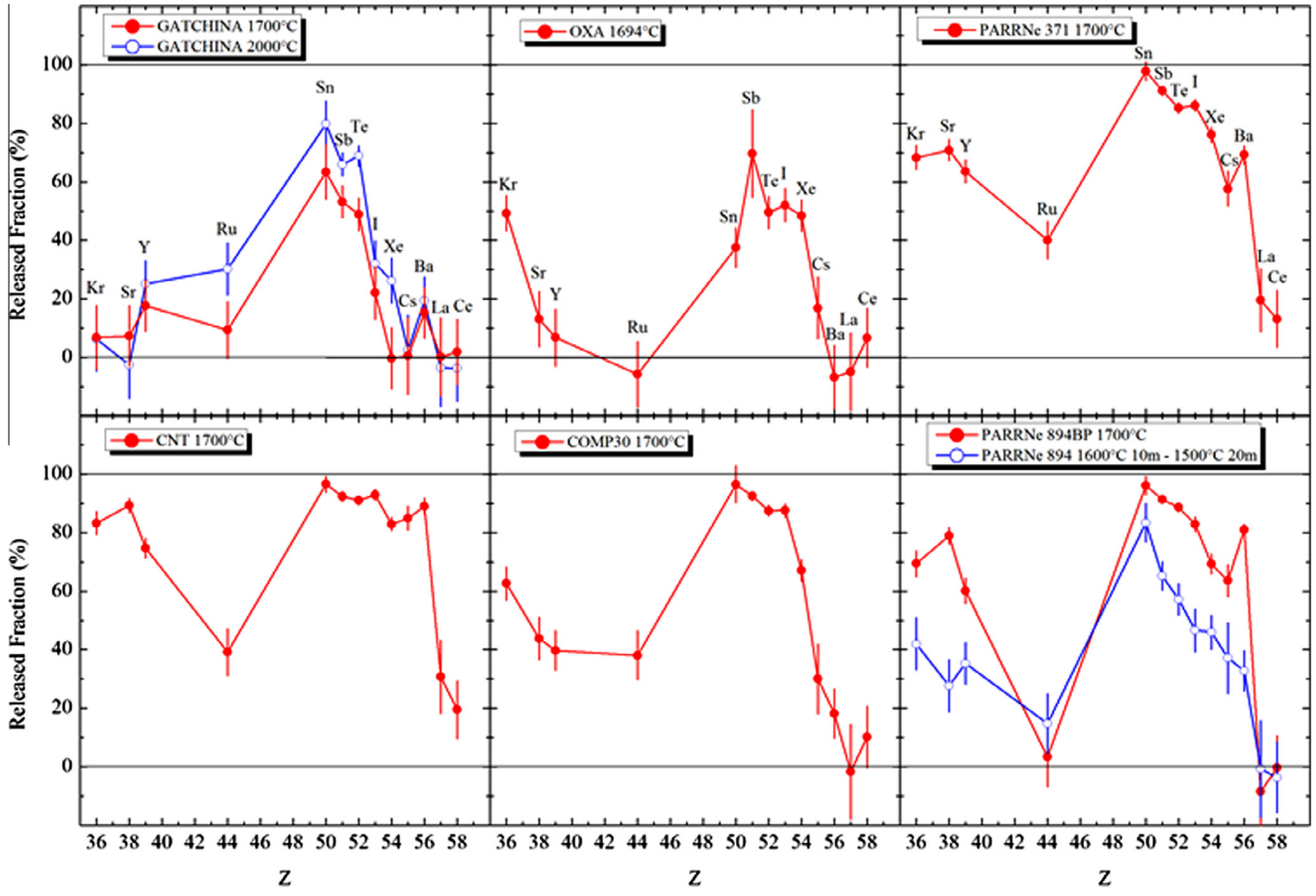

Fig. 9. Released fractions from the seven samples of uranium carbide as a function of the atomic number.

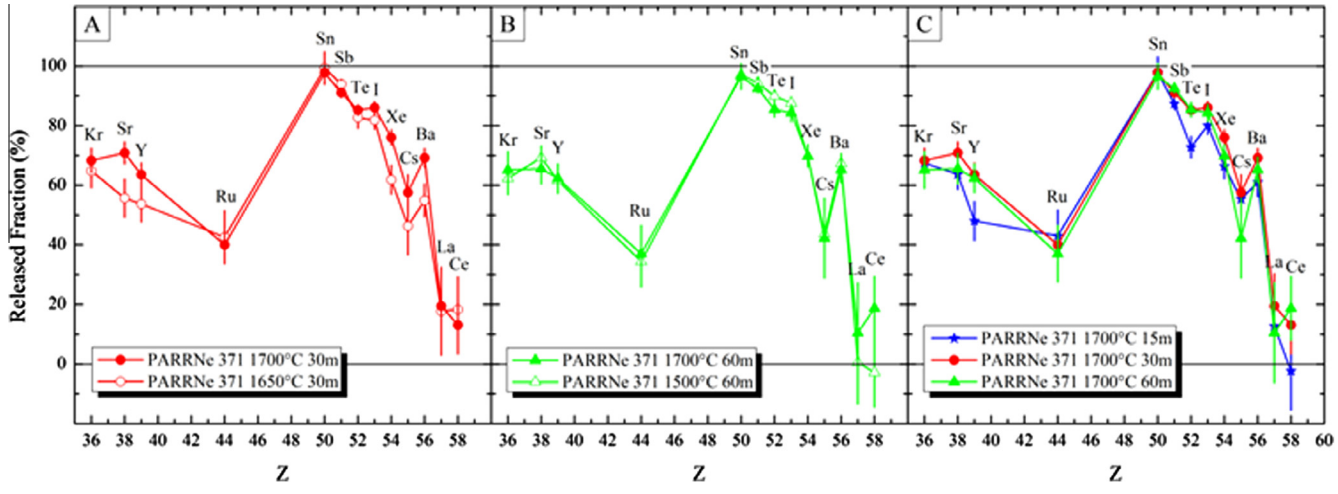

Fig. 10. Released fractions from PARRNe 371 samples for different heating temperatures and heating times.

the different samples according to their release properties: the CNT sample appears to be the best one, followed by PARRNe 894BP and 371, then COMP30, PARRNe 894, OXA and finally GATCHINA.

In Fig. 12, the RF of all the studied elements excepted La, Ce and Ru (the most release-resistant elements of our study) is plotted as a function of the open porosity of the samples.

The open porosity clearly appears to be a determining factor for high release of radioisotopes, even if this observation has to be moderated for COMP30 and PARRNe 894.

Indeed, the GATCHINA samples with P_{open} = 5% release only the elements for which the predominant release process is effusion or desorption. This is followed by the OXA samples with P_{open} = 26%, which are as well poorly efficient in terms of release. On the contrary, the CNT sample with P_{open} = 77% shows the best release results. A large open porosity seems to be associated with a high UC_2 fraction. OXA and GATCHINA, unlike all the other samples, are mainly made of UC and both have the lowest porosity values. On the other hand, COMP30, obtained like OXA from uranium

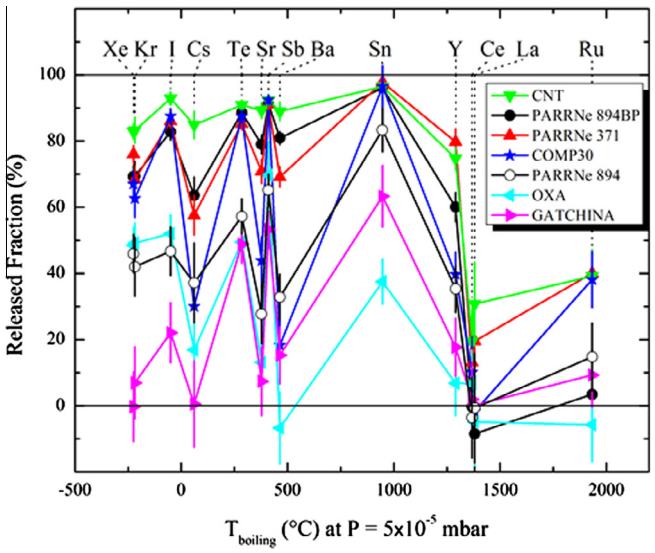

Fig. 11. Released fractions from the UC_x samples as a function of the boiling temperature of each species at 5×10^{-5} mbar calculated from Lide [35].

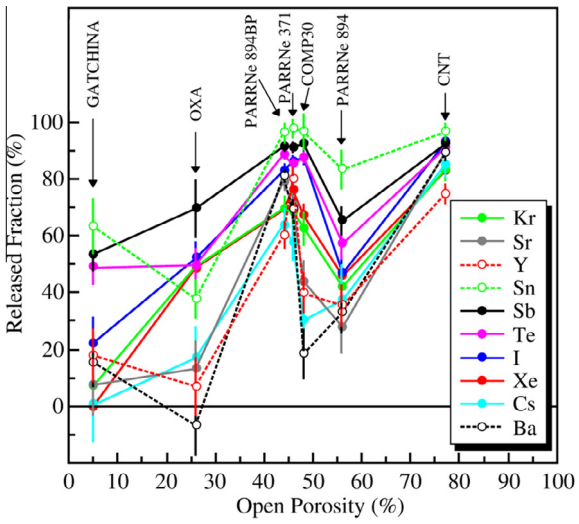

Fig. 12. Released fraction as a function of the open porosity for the seven kinds of samples.

oxalate but with UC_2 as main phase, has an open porosity value very similar to that of the PARRNe 371, 894 and 894BP samples.

The samples having an open porosity of about 50%, i.e. COMP30, PARRNe 371, PARRNe 894 and PARRNe 894BP, except for PARRNE 894BP, exhibit large pores in the 100 μm range (see Fig. 2). Their large distribution of pore sizes can be explained by a heterogeneous microstructure, as clearly revealed by the SEM observations for COMP30 (cracks on surface) and PARRNe 894 (the most heterogeneous PARRNe samples). Among these three samples, PARRNe 371 is the most homogeneous one and shows high RF. As for PARRNe 894BP, although it is the less porous in this group (P_{open} = 44%), it displays a more uniform pore size distribution (~5 μm) and its release properties are very similar to those of PARRNe 371.

Therefore, it appears that in order to exhibit good release properties, a sample must have the following characteristics: high porosity and small pore size with a uniform distribution. In the present study, the CNT sample combines some of these criteria (highest open porosity and narrowest pore size distribution) and presents actually the largest released fractions.

In the context of the studies of fuel's performances, it was mentioned that high porosity fuel releases more fission gas than high density one which retains gas that precipitates in fine bubble into the matrix [36]. In PARRNe-type samples, COMP30 and CNT, hypostoichiometric UC_2 is stabilized, inducing the formation of vacancies in UC_{2-x} phase in which FP can be trapped. Nevertheless it was also reported that pores and grain boundaries aid in increasing the release of fission gas, allowing individual grains to swell and gas bubbles to interconnect [37,38]. When limiting the grain size in UC_x as performed for PARRNe 894BP, compared to PARRNNe 894, and in CNT sample (10 min of carburization limiting the grain growth), FP release would be favored.

The correlation between the open porosity and the oxygen content, as it was studied in uranium–plutonium carbide fuels [24], could be discussed by a careful study of our XRD results. It was shown that the higher the oxygen content, the lower the sintered density, meaning that in our study a high level of oxygen content would be helpful. In OXA and GATCHINA, no carbon was added in excess; the impurities, and in particular oxygen that cannot be excluded regarding to the synthesis method, can be trapped into the carbide leading to a higher cell parameter (Table 4). Carbon in excess in COMP30 and PARRNe-type samples could allow the degassing of oxygen into CO leading to stoichiometric UC (not observed experimentally, see Table 4) and higher open pore volume per gram and total pore area (experimentally observed, see Table 6). However, the difference in term of porosity and density is probably due to the stabilization of UC_2 (less dense) instead of UC and unreacted carbon rather than an oxygen content effect that may be negligible.

Recently, porous structures with nanotubes were investigated in the frame of the the SPES-target research and development [4]. The main difference in the preparation of the samples is the heating time of sintering: 20 min in our work compared to 39 h [4]. However, the resulting microstructure is similar to ours, porous (about 75%) and heterogeneous, with micrometric aggregates of UC_x and nanometric UC_x grains growing on carbon nanotubes. For target temperatures equal to 1600 and 1800 °C, the Sr and Sn releases have been found to be faster with CNT than with standard UC_x, which is in agreement with our results at 1700 °C. But the gain in the release properties was not fully confirmed at 2000 °C and the yields were found to be, for most isotopes, lower than those obtained with a standard UC_x target. This raises the question of the stability of the microstructure of the CNT sample heated at high temperature for a long time.

Previous experimental studies as well as simulations of diffusion and effusion in UC_x pellets, showed the effect of the grain size on the release efficiency. On the one hand, yields of Cs and Fr isotopes were measured higher using high density UC target material with a grain size of 5 μm instead of 20 μm [12]. On the other hand, for elements having short sticking times, the calculated release efficiency presents a maximum when the UC-grain diameter is below 1 μm; for elements with medium and long sticking times, the optimal grain size is found to be in the 1–10 μm range [39,40]. The grain size distributions observed in our study are not sufficiently homogeneous to highlight a correlation between the grain size and the release properties, but behavior differences between elements with long (Sn) or short (Kr) sticking time were identified.

Questions on nanostructured UC_x prototypes are being currently addressed. Homogeneous and nanostructured samples have successfully been synthesized and recently a full target was tested on-line at ISOLDE with promising results [A. Gottberg et al. in preparation]. New synthesis developments are in progress to obtain nanostructured samples, using nanopowders of uranium

dioxide (obtained by planetary milling) or oxalate and MWCNT. The controlled nanostructure, achieved by sintering a homogeneous mixture, is being compared to the conventional ones tested up to now in order to quantify the improvement in terms of fission-product releases and to answer the following questions: what is the benefit of a homogeneous nanostructure versus a heterogeneous microstructure commonly used at ISOL facilities? What is the impact of the nature of both, the uranium nanopowder and of the source of carbon? The results obtained will help us to confirm the role of the homogeneity of the pellet, the advantage of a nanostructure (versus its expected disadvantage, the increase of its pyrophoricity) and to corroborate the impact of the density of the target.

5. Conclusion

Results of this experimental method are of great use to improve the performance of the various ISOL-type facilities worldwide. Two experiments have been successfully achieved. The first demonstrated the feasibility of the experimental method and the second (this study) provided results at higher temperatures (1700 °C and 2000 °C) on seven very different uranium carbide composites, for instance the conventional material used at the ALTO facility, high density monocarbides and very porous and less dense composites containing multi-walled carbon nanotubes.

Improvements on the irradiation station, sample holder and fast furnace allow us to collect reproducible and conclusive results of release properties. XRD analysis revealed the phase quantities and assisted the calculation of densities and porosities of the samples. An exhaustive assessment of the microstructure is proposed by combining SEM and Hg porosimetry. The correlation between the physicochemical properties and the released fractions shows that the open porosity is the factor with the greatest impact on the release efficiency. The homogeneity of the microstructure and the pore size distribution contribute significantly to the increase of the release. Even if the homogeneity of the microstructure that is required for conclusive results was not yet achieved, the use of carbon nanotubes in place of graphite appears to be promising.

Acknowledgments

The authors would like to thank the members of the ALTO facility for delivering the deuteron beam and for their technical assistance during the experiment, as well as S. Wurtz and N. Decovemacker for their support for nuclear and radiation protection. We also thank M. Mahoudeaux for her involvement in the project from April to July 2013 during her internship. The financial support of the European Community under FP7 ENSAR-ActILab (contract number 262010) is highly acknowledged.

References

[1] G.A. Cowan, C.J. Orth, Diffusion of fission products at high temperatures from refractory matrices, in: Second United Nations International Conference on the Peaceful Uses of Atomic Energy, A/CONF.15/P/613, USA, June 1958.
[2] L.C. Carraz, I.R. Haldorsen, H.L. Ravn, M. Skarestad, L. Westgaard, Fast release of nuclear reaction products from refractory matrices, Nucl. Instr. Meth. B 148 (1978) 217–230.
[3] P. Hoff, O.C. Jonsson, E. Kugler, H.L. Ravn, Release of nuclear products from refractory compounds, Nucl. Instr. Meth. B 221 (1984) 313–329.
[4] S. Corradetti, L. Biasetto, M. Manzolaro, D. Scarpa, S. Carturan, A. Andrighetto, G. Prete, J. Vasquez, P. Zanonato, P. Colombo, C.U. Jost, D.W. Stracener, Neutron-rich isotope production using a uranium carbide – nanotubes SPES target prototype, Eur. Phys. J. A 49–56 (2013).
[5] K. Tshoo, D.Y. Jang, H.J. Woo, B.H. Kang, G.D. Kim, W. Hwang, Y.K. Kim, Design study of 10 kW direct fission target for RISP project, EPJ Web Conf. 66 (2014) 11016.
[6] O. Bajeat, P. Delahaye, C. Couratin, M. Dubois, H. Franberg-Delahaye, J.L. Henares, Y. Huguet, P. Jardin, N. Lecesne, P. Lecomte, R. Leroy, L. Maunoury, B. Osmond, M. Sjodin, Development of target ion source systems for radioactive beams at GANIL, Nucl. Instr. Meth. B 317 (2013) 411–416.
[7] B. Hy, N. Barré-Boscher, A. Özgümüs, B. Roussière, S. Tusseau-Nenez, C. Lau, M. Cheikh Mhamed, M. Raynaud, A. Said, K. Kolos, E. Cottereau, S. Essabaa, O. Tougait, M. Pasturel, An off-line method to characterize the fission product release from uranium carbide-target prototypes developed for SPIRAL2 project, Nucl. Instr. Meth. B 288 (2012) 34–41.
[8] M. Lebois, P. Bricault, Simulations for the future converter of the e-linac for the TRIUMF ARIEL facility, J. Phys. Conf. Ser. 312 (2011) 052013.
[9] G. Lhersonneau, O. Alyakrinskiy, O. Bajeat, A.E. Barzakh, M. Dubois, C. Eléon, S. Essabaa, D.V. Fedorov, G. Gaubert, A.M. Ionan, V.S. Ivanov, P. Jardin, A. Lanchais, C. Lau, R. Leroy, K.A. Mezilev, M. Cheikh Mhamed, F.V. Moroz, S.Yu. Orlov, V.N. Panteleev, V. Rizzi, B. Roussière, M.G. Saint Laurent, L. Stroe, L.B. Tecchio, A.C.C. Villari, Yu.M. Volkov, Tests of high-density UC targets developed at GATCHINA for neutron-rich radioactive-beam facilities, Nucl. Instr. Meth. B 266 (2008) 4326–4329.
[10] V.N. Panteleev, O. Alyakrinskiy, M. Barbui, A.E. Barzakh, M. Dubois, C. Eleon, S. Essabaa, D.V. Fedorov, G. Gaubert, A.M. Ionan, V.S. Ivanov, P. Jardin, C. Lau, R. Leroy, G. Lhersonneau, K.A. Mezilev, M.C. Mhamed, P.L. Molkanov, F.V. Moroz, S.Yu. Orlov, M.G. Saint Laurent, L. Stroe, L.B. Tecchio, M. Tonezzer, A.C.C. Villar, Yu.M. Volkov, Studies of uranium carbide targets of a high density, Nucl. Instr. Meth. B 266 (2008) 4247–4251.
[11] V.N. Panteleev, A.E. Barzakh, S. Essabaa, D.V. Fedorov, A.M. Ionan, V.S. Ivanov, C. Lau, R. Leroy, G. Lhersonneau, K.A. Mezilev, P.L. Molkanov, F.V. Moroz, S. Yu Orlov, L. Stroe, L.B. Tecchio, A.C.C. Villari, Yu.M. Volkov, Electron beam-plasma ionizing target for the production of neutron-rich nuclides, Nucl. Instr. Meth. B 266 (2008) 4294–4297.
[12] V. Panteleev, O. Alyakrinskiy, M. Barbui, A. Barzakh, D. Fedorov, V. Ivanov, G. Lhersonneau, K. Mezilev, P. Molkanov, F. Moroz, S. Orlov, L. Stroe, L. Tecchio, M. Tonezzer, Y. Volkov, Production of Cs and Fr isotopes from a high-density UC targets with different grain dimensions, Eur. Phys. J. A 42 (2009) 495–501.
[13] S. Fernandes, R. Bruetsch, R. Catherall, F. Groeschel, I. Guenther-Leopold, J. Lettry, E. Manfrin, S. Marzari, E. Noah, S. Sgobba, T. Stora, L. Zanini, Microstructure evolution of nanostructured and submicrometric porous refractory ceramics induced by a continuous high-energy proton beam, J. Nucl. Mater. 416 (2011) 99–110.
[14] J.P. Ramos, A. Gottberg, T.M. Mendonça, C. Seiffert, A.M.R. Senos, H.O.U. Fynbo, O. Tengblad, J.A. Briz, M.V. Lund, G.T. Koldste, M. Carmona-Gallardo, V. Pesudo, T. Stora, Intense $^{31-35}$Ar beams produced with a nanostructured CaO target at ISOLDE, Nucl. Instr. Meth. B 320 (2014) 83–88.
[15] J. Guillot, Internship M2, CERN (2014).
[16] L. Lutterotti, Total pattern fitting for the combined size-strain-stress-texture determination in thin film diffraction, Nucl. Instr. Meth. B 268 (2010) 334–340.
[17] L. Lutterotti, M. Bortolotti, Object oriented programming and fast computation techniques in Maud, a program for powder diffraction analysis written in java, IUCr Compcomm Newslett. 1 (2003) 43–50.
[18] S. Grazulis, D. Chateigner, R.T. Downs, A.F.T. Yokochi, M. Quiros, L. Lutterotti, E. Manakov, J. Butkus, P. Moeckg, A. Le Bail, Crystallography open database – an open-access collection of crystal structures, Appl. Crystallogr. 42 (2009) 726–729.
[19] K.K. Aligizaki, Pore Structure of Cement-Based Materials: Testing, Interpretation and Requirements, Modern Concrete Technology 12, Taylor & Francis, Abingdon, 2006.
[20] S. Lowell, J.E. Shields, M.A. Thomas, M. Thommes, Characterization of porous solids and powders: surface area, pore size and density, Particle Technology Series, vol. 16, Springer Science Business Media, LLC, 2004.
[21] N. Hingant, N. Clavier, N. Dacheux, N. Barre, N. Hubbert, S. Obbade, S. Taborda, F. Abraham, Preparation, sintering and leaching of optimized uranium thorium dioxides, J. Nucl. Mater. (2009) 385–400.
[22] N. Hingant, N. Clavier, N. Dacheux, S. Hubert, N. Barré, R. Podor, L. Aranda, Preparation of morphology controlled $Th_{(1-x)}U_xO_2$ sintered pellets from low-temperature precursors, Powder Technol. 208 (2011) 454–460.
[23] L. Biasetto, S. Carturan, G. Maggioni, P. Zanonato, P. Di Bernardo, P. Colombo, A. Andrighetto, G. Prete, Fabrication of mesoporous and high specific surface area lanthanum carbide–carbon nanotube composites, J. Nucl. Mater. 385 (2009) 582–590.
[24] C. Duguay, G. Pelloquin, Fabrication of mixed uranium–plutonium carbide fuel pellets with a low oxygen content and an open-pore microstructure, J. Eur. Ceram. Soc. 35 (2015) 3977–3984.
[25] A.E. Austin, Carbon positions in uranium carbides, Acta Crystallogr. 12 (1959) 159.
[26] P.Y. Chevalier, E. Fischer, Thermodynamic modelling of the C–U and B–U binary systems, J. Nucl. Mater. 288 (2001) 100–129.
[27] D. Manara, F. De Bruycker, A.K. Sengupta, R. Agarwal, H.S. Kamath, Thermodynamic and thermophysical properties of the actinide carbides, in: R.J.M. Konings (Ed.), Comprehensive Nuclear Materials, vol. 2, Elsevier, Oxford, 2012, pp. 87–137.
[28] J. Fayos, Possible 3D carbon structures as progressive intermediates in graphite to diamond phase transition, J. Sol. State Chem. 148 (1999) 278–285.
[29] B.T.M. Willis, Structures of UO_2, UO_{2+x} and U_4O_9 by neutron diffraction, J. Phys. 25 (1964) 431–439.
[30] L.B. McCusker, R.B. Von Dreele, D.E. Cox, D. Louer, P. Scardi, Rietveld refinement guidelines, J. Appl. Crystallogr. 32 (1999) 36–50.
[31] B.H. Toby, R factors in Rietveld analysis: how good is good enough?, Powder Diffr 21 (2006) 67–70.

[32] H. Tagawa, K. Fujii, Formation of U_2C_3 in the reaction of UC_2 with UO_2, J. Nucl. Mater. 39 (1971) 109–114.
[33] J.W. Arblaster, Vapour pressure equations for the platinum group elements, Platinum Met. Rev. 51 (3) (2007) 130–135.
[34] B. Roussière, O. Bajeat, N. Barré, C. Bourgeois, F. Clapier, E. Cottereau, C. Donzaud, M. Ducourtieux, S. Essabaa, D. Guillemaud-Mueller, F. Ibrahim, C. Lau, F. Le Blanc, H. Lefort, C.F. Liang, A.C. Mueller, J. Obert, N. Pauwels, J.C. Potier, F. Pougheon, J. Proust, J. Sauvage, O. Sorlin, D. Verney, A. Wojtasiewicz, Release of Kr, Ag, Sn, I and Xe from UC_x targets, Nucl. Instr. Meth. B 246 (2006) 288–296.
[35] D.R. Lide, CRC Handbook of Chemistry and Physics, eighty fifth ed., CRC Press, Boca Raton, FL, 2004–2005.
[36] G.M. Nickerson, W.E. Kastenberg, Preliminary assessments of carbide fuel pins during mild overpower transients in LMFBRs, Nucl. Eng. Des. 36 (1976) 209–233.
[37] T. Preusser, Modeling of carbide fuel rods, Nucl. Technol. 57 (1982) 343–371.
[38] L.H. Hallman, Advanced fuels modeling: evaluating the steady-state performance of carbide fuel in helium-cooled reactors using FRAPCON 3.4 (Master of Science in Nuclear Engineering), University of South Carolina, 2013.
[39] M. Golkovsky, K. Gubin, O. Alyakrinsky, S. Bardakhanov, About carbides–made nanoceramics fission target for RIB production, in: Proceedings of EPAC08 Genova, Italy, 268–270, 2008.
[40] O. Alyakrinskiy, K. Gubin, P. Martyshkin, L. Tecchio, Influence of grain size and porosity on the release of radioactive isotopes from target materials with high open porosity, Nucl. Instr. Meth. B 267 (2009) 2554–2558.